J|A|C|S
ARTICLES
Published on Web 05/12/2006

Relaxation Rates of Degenerate ^{1}H Transitions in Methyl Groups of Proteins as Reporters of Side-Chain Dynamics

Vitali Tugarinov and Lewis E. Kay*

Contribution from the Departments of Medical Genetics, Biochemistry, and Chemistry, University of Toronto, Toronto, Ontario, Canada M5S 1A8

Received February 2, 2006; E-mail: kay@pound.med.utoronto.ca

Abstract: Experiments for quantifying the amplitudes of motion of methyl-containing side chains are presented that exploit the rich network of cross-correlated spin relaxation interactions between intra-methyl dipoles in highly deuterated, selectively $^{13}CH_2D$- or $^{13}CH_3$-labeled proteins. In particular, the experiments measure spin relaxation rates of degenerate ^{1}H transitions in methyl groups that, for high-molecular-weight proteins, are very simply related to methyl three-fold symmetry axis order parameters. The methodology presented is applied to studies of dynamics in a pair of systems, including the 7.5-kDa protein L and the 82-kDa enzyme malate synthase G. Good agreement between ^{1}H- and ^{2}H-derived measures of side-chain order are obtained on highly deuterated proteins with correlation times exceeding approximately 10 ns (correlation coefficients greater than 0.95). Although ^{2}H- and ^{13}C-derived measures of side-chain dynamics are still preferred, the present work underscores the potential of using ^{1}H relaxation for semiquantitative estimates of methyl side-chain flexibility, while the high level of consistency between the different spin probes of motion establishes the reliability of the dynamics parameters.

Introduction

A complete description of molecular structure is based not only on static molecular images obtained by X-ray diffraction, NMR spectroscopy, and now cryo-EM techniques[1−3] but must also include information that relates to how conformations change in time due to molecular dynamics.[4−6] In this regard, NMR spectroscopy has emerged as a valuable probe since experiments have been developed that can be used to study motion over a very broad range of time scales.[7−10] One of the most interesting and important areas of study as related to proteins involves side-chain dynamics that play an important role in stability, molecular recognition, catalysis, and ligand binding.[11−15] Over the past decade, NMR experiments for the study of such motional processes have emerged,[12,16−22] in addition to new computational approaches that incorporate "dynamic" information into the calculation of protein structures.[23]

NMR studies of side-chain dynamics frequently make use of the deuteron as a spin-spy probe of motion since ^{2}H spin relaxation is dominated by the well-understood quadrupolar interaction.[24] Initial studies focused on uniformly ^{13}C-labeled molecules that were fractionally deuterated, where $^{13}CH_2D$ isotopomers were selected as reporters of motion in methyl-containing side-chains[16,19] or where ^{13}CHD spin systems were used in the study of other side-chain sites.[17] In applications involving larger proteins, such as the 723-residue malate synthase G (MSG, 82 kDa), new labeling schemes can be employed that make use of commercially available precursors resulting in 100% incorporation of $^{13}CH_2D$ groups at Ile(δ1), Leu, and Val methyl sites, and we have recently described a dynamics study involving Ile(δ1) $^{13}CH_2D$ probes in MSG.[20] This labeling approach leads to significant increases in sensitivity that are critical for applications to high-molecular-weight proteins. It has also been shown that, for large proteins such as

(1) Riekel, C.; Burghammer, M.; Schertler, G. *Curr. Opin. Struct. Biol.* **2005**, *15*, 556−562.
(2) Bax, A.; Grishaev, A. *Curr. Opin. Struct. Biol.* **2005**, *15*, 563−570.
(3) Jiang, W.; Ludtke, S. J. *Curr. Opin. Struct. Biol.* **2005**, *15*, 571−577.
(4) Karplus, M.; McCammon, J. A. *Annu. Rev. Biochem.* **1983**, *53*, 263−300.
(5) Frauenfelder, H.; Sligar, S. G.; Wolynes, P. G. *Science* **1991**, *254*, 1598−1603.
(6) Kern, D.; Zuiderweg, E. R. *Curr. Opin. Struct. Biol.* **2003**, *13*, 748−757.
(7) Peng, J. W.; Wagner, G. *Methods Enzymol.* **1994**, *239*, 563−596.
(8) Kay, L. E. *Nat. Struct. Biol. NMR Suppl.* **1998**, *5*, 513−516.
(9) Ishima, R.; Torchia, D. A. *Nat. Struct. Biol.* **2000**, *7*, 740−743.
(10) Palmer, A. G.; Kröenke, C. D.; Loria, J. P. *Methods Enzymol.* **2001**, *339*, 204−238.
(11) Lee, A. L.; Wand, A. J. *Nature* **2001**, *411*, 501−504.
(12) Mulder, F. A. A.; Mittermaier, A.; Hon, B.; Dahlquist, F. W.; Kay, L. E. *Nat. Struct. Biol.* **2001**, *8*, 932−935.
(13) Tugarinov, V.; Kay, L. E. *Biochemistry* **2005**, *44*, 15970−15977.
(14) Eisenmesser, E. Z.; Millet, O.; Labeikovsky, W.; Korzhnev, D. M.; Wolf-Watz, M.; Bosco, D. A.; Skalicky, J. J.; Kay, L. E.; Kern, D. *Nature* **2005**, *3*, 117−121.
(15) Kay, L. E.; Muhandiram, D. R.; Wolf, G.; Shoelson, S. E.; Forman-Kay, J. D. *Nat. Struct. Biol.* **1998**, *5*, 156−163.
(16) Muhandiram, D. R.; Yamazaki, T.; Sykes, B. D.; Kay, L. E. *J. Am. Chem. Soc.* **1995**, *117*, 11536−11544.
(17) Yang, D.; Mittermaier, A.; Mok, Y. K.; Kay, L. E. *J. Mol. Biol.* **1998**, *276*, 939−954.
(18) Ishima, R.; Louis, J. M.; Torchia, D. A. *J. Am. Chem. Soc.* **1999**, *121*, 11589−11590.
(19) Millet, O.; Muhandiram, D. R.; Skrynnikov, N. R.; Kay, L. E. *J. Am. Chem. Soc.* **2002**, *124*, 6439−6448.
(20) Tugarinov, V.; Ollerenshaw, J. E.; Kay, L. E. *J. Am. Chem. Soc.* **2005**, *127*, 8214−8225.
(21) LeMaster, D. M.; Kushlan, D. M. *J. Am. Chem. Soc.* **1996**, *118*, 9255−9264.
(22) Jin, C.; Prompers, J. J.; Brüschweiler, R. *J. Biomol. NMR.* **2003**, *26*, 241−217.
(23) Lindorff-Larsen, K.; Best, R. B.; Depristo, M. A.; Dobson, C. M.; Vendruscolo, M. *Nature* **2005**, *433*, 128−132.
(24) Abragam, A. *Principles of Nuclear Magnetism*; Clarendon Press: Oxford, 1961; Chapter VIII.

MSG, it is possible to extract reliable values of methyl side-chain order parameters, S_{axis}, through measurement of ^2H transverse relaxation rates in $^{13}CHD_2$ methyl groups that can also be prepared at "100% abundance" in proteins through the use of suitable precursors.[20] The availability of $^{13}CHD_2$ probes also facilitates measurement of dynamics through the use of complementary approaches that quantify ^{13}C relaxation,[13,25] without concern about $^1H-^{13}C$ cross-correlation effects that complicate both the experiments and their subsequent analysis in the case of ^{13}C T_1 and T_2 relaxation studies involving $^{13}CH_3$ and $^{13}CH_2D$ methyl groups.[26] Excellent agreement has been obtained between S^2_{axis} values measured from ^2H ($^{13}CH_2D$, $^{13}CHD_2$)- and ^{13}C ($^{13}CHD_2$)-based experiments in the work from our laboratory on MSG,[13] and Torchia and co-workers have also reported a good correlation between ^2H- and ^{13}C-derived measures of order in studies on the HIV-protease.[25]

^1H spin relaxation in methyl groups is, of course, also sensitive to S^2_{axis}, and it should be possible, in principle, to develop ^1H-based relaxation experiments that provide robust measures of order. However, studies involving ^1H relaxation are, in general, qualitative at best. The main complication in the extraction of accurate dynamic parameters results from contributions to relaxation from neighboring protons (in the present case, external to the methyl group in question) that can be very significant and that are difficult to account for in a quantitative manner; any experimental approach must effectively solve this problem, and to our knowledge this remains an outstanding issue. For example, while Ishima et al. report a correlation of 0.95 between measured methyl ^{13}C and ^2H transverse relaxation rates in HIV-protease, the correlation drops to 0.81 when ^2H and ^1H rates are compared.[25] We show here that nearly quantitative measures of methyl side-chain dynamics can be obtained via measurement of ^1H relaxation rates in $^{13}CH_2D$ and $^{13}CH_3$ methyl groups of highly deuterated proteins by exploiting the presence of more than one proton in such moieties. In particular, cross-correlation effects that derive from the presence of multiple proton spins lead to differences in relaxation of degenerate ^1H transitions in both $^{13}CH_2D$ and $^{13}CH_3$ spin systems.[27−29] Such differences can be "put to use" to effectively subtract out relaxation interactions resulting from proximal ^1H spins. NMR experiments are presented for measuring transverse relaxation rates of individual ^1H transitions in $^{13}CH_2D$ and $^{13}CH_3$ methyl groups of proteins and simple expressions that relate S^2_{axis} to the difference in measured rates are derived. Values of S^2_{axis} obtained in studies of both the 7.5-kDa protein L[30] and the 82-kDa MSG[31] are shown to be in good agreement with ^2H-derived measures of order.

Materials and Methods

NMR Samples. Relaxation rates of degenerate proton transitions in $^{13}CH_2D$ methyl groups were measured on {U-[^{15}N,^2H], Ileδ1-[$^{13}CH_2D$]}-MSG, while studies involving $^{13}CH_3$ probes of side-chain dynamics were performed on {U-[^{15}N,^2H], Ileδ1-[$^{13}CH_3$], Leu,Val-[$^{13}CH_3$,$^{12}CD_3$]}-labeled MSG and a {U-[^{15}N,^2H], Ileδ1-[$^{13}CH_3$], Leu, Val-[$^{13}CH_3$,$^{12}CD_3$]}-labeled sample of the B1 immunoglobulin binding domain of peptostreptoccocal protein L. All the samples were prepared as described in detail previously[32,33] using U-[^2H]-D-glucose as the main carbon source and appropriate α-keto-acid precursors for selective methyl labeling.[34] We have chosen also to include ^{15}N labeling so that $^1H-^{15}N$ correlation maps could be obtained, if desired, by dissolving samples in H_2O. The MSG samples comprised 99.9% D_2O, 25 mM sodium phosphate, pH 7.1 (uncorrected), 20 mM $MgCl_2$, 0.05% NaN_3, and 5 mM DTT and were 0.7 mM (Ileδ1-[$^{13}CH_2D$]) and 0.5 mM (Ileδ1-[$^{13}CH_3$], Leu,Val-[$^{13}CH_3$,$^{12}CD_3$]) in protein. The protein L sample was 1.4 mM in protein, 99.9% D_2O, 50 mM sodium phosphate, pH 6.0 (uncorrected).

NMR Spectroscopy. NMR experiments were performed at 500 (600) MHz, using Varian Inova spectrometers equipped with room-temperature (cryogenically cooled) triple-resonance probes. Data sets for MSG and protein L were recorded at 37 and 5 °C, respectively. Spectra obtained with the pulse scheme of Figure 2a ({U-[^{15}N,^2H], Ileδ1-[$^{13}CH_2D$]}-MSG) had acquisition times of 80 (64) ms in t_1 (t_2). Values of $R^F_{2,H}$ ($R^S_{2,H}$) relaxation rates were recorded with parametrically varied delays T (Figure 2a) of 0, 4, 8, 12, and 16 (0, 4, 8, 12, 16, 20, 24, 28, and 32) ms (i.e., T set to a multiple of $1/(2^1J_{CH})$, with $^1J_{CH}$ measured to be 125.1 ± 0.4 Hz in $^{13}CH_2D$ isotopomers[35]). A number of postacquisition data manipulations in the $^{13}CH_2D$-TROSY-derived experiment (Figure 2a) have been performed as described in detail previously[20,36] and are briefly summarized in the Results and Discussion section below. Unique to the present experiment is that data sets acquired with $T = k/^1J_{CH}$ and with $T = (2k + 1)/(2^1J_{CH})$, where $k = 0$, 1, 2, ..., are out of phase with respect to each other by 90° in the F_2 dimension and must, therefore, be phased separately to pure absorptive line shapes. In addition, each data set acquired with $k = 1$, 3, 5, ... is 180° out of phase with respect to matrices for which $k = 0$, 2, 4, ...; each data set for which negative correlations are obtained is phased by 180° (in one of F_1/F_2, see below) prior to fitting peak intensities to a monoexponential decay function, $A_0\, e^{-RT}$, where R is the relaxation rate and T the relaxation delay (see Results and Discussion for the details of experiments).

$R^S_{2,H}$, $R^F_{2,H}$ relaxation rates of degenerate ^1H transitions in [$^{13}CH_3$]-labeled samples have been measured with the sequences of Figure 4a,b, respectively. Acquisition times of 47 (64) and 64 (64) ms in t_1 (t_2) have been used in studies of {U-[^{15}N,^2H], Ileδ1-[$^{13}CH_3$], Leu,Val-[$^{13}CH_3$,$^{12}CD_3$]}-MSG and {U-[^{15}N,^2H], Ileδ1-[$^{13}CH_3$], Leu,Val-[$^{13}CH_3$,$^{12}CD_3$]}-protein L, respectively. $R^F_{2,H}$ ($R^S_{2,H}$) rates were recorded with parametrically varied delays T (Figure 4a,b) of 0.7, 1, 1.5, 2, 2.5, 3, 4, and 5 (0.7, 5, 10, 15, 20, 25, 30, and 40) ms for {U-[^{15}N,^2H], Ileδ1-[$^{13}CH_3$], Leu,Val-[$^{13}CH_3$,$^{12}CD_3$]}-MSG, and with 1.1, 5, 10, 15, 20, 25, 30, and 35 (1.1, 25, 50, 75, 100, and 150) ms for {U-[^{15}N,^2H], Ileδ1-[$^{13}CH_3$], Leu,Val-[$^{13}CH_3$,$^{12}CD_3$]}-protein L. $R^F_{2,H}/R^S_{2,H}$ rates were obtained by fitting peak intensities to monoexponential decay functions, as in studies involving $^{13}CH_2D$ methyls.

All NMR spectra were processed using the NMRPipe/NMRDraw suite of programs and associated software.[37] Errors in the fitted relaxation rates were estimated by a Monte Carlo analysis[38] using random noise in the spectra as an estimate of experimental uncertainties in peak intensities. Average errors of 1.1 (0.6), 2.1 (1.6), and 3.1 (1.0)% have been obtained for $R^F_{2,H}$ ($R^S_{2,H}$) rates in protein L, {U-[^{15}N,^2H],

(25) Ishima, R.; Petkova, A. P.; Louis, J. M.; Torchia, D. A. *J. Am. Chem. Soc.* **2001**, *123*, 6164−6171.
(26) Kay, L. E.; Torchia, D. A. *J. Magn. Reson.* **1991**, *95*, 536−547.
(27) Werbelow, L. G.; Marshall, A. G. *J. Magn. Reson.* **1973**, 299−313.
(28) Kay, L. E.; Prestegard, J. H. *J. Am. Chem. Soc.* **1987**, *109*, 3829−3835.
(29) Müller, N.; Bodenhausen, G.; Ernst, R. R. *J. Magn. Reson.* **1987**, *75*, 297−334.
(30) Scalley, M. L.; Yi, Q.; Gu, H.; McCormack, A.; Yates, J. R.; Baker, D. *Biochemistry* **1997**, *36*, 3373−82.
(31) Howard, B. R.; Endrizzi, J. A.; Remington, S. J. *Biochemistry* **2000**, *39*, 3156−68.
(32) Tugarinov, V.; Kay, L. E. *J. Biomol. NMR* **2004**, *28*, 165−172.
(33) Korzhnev, D. M.; Kloiber, K.; Kanelis, V.; Tugarinov, V.; Kay, L. E. *J. Am. Chem. Soc.* **2004**, *126*, 3964−3973.
(34) Tugarinov, V.; Kay, L. E. *Chembiochem* **2005**, *6*, 1567−1577.
(35) Mittermaier, A.; Kay, L. E. *J. Biomol. NMR* **2002**, *23*, 35−45.
(36) Ollerenshaw, J. E.; Tugarinov, V.; Skrynnikov, N. R.; Kay, L. E. *J. Biomol. NMR* **2005**, *33*, 25−41.
(37) Delaglio, F.; Grzesiek, S.; Vuister, G. W.; Zhu, G.; Pfeifer, J.; Bax, A. *J. Biomol. NMR* **1995**, *6*, 277−293.
(38) Kamith, U.; Shriver, J. W. *J. Biol. Chem.* **1989**, *264*, 5586−5592.

Ileδ1-[$^{13}CH_2D$]}-MSG, and {U-[^{15}N,^2H], Ileδ1-[$^{13}CH_3$], Leu,Val-[$^{13}CH_3$,$^{12}CD_3$]}-MSG, respectively.

Rotational Diffusion of Protein L and MSG. The molecular tumbling correlation times of protein L (at 5 °C) and MSG (at 37 °C), D_2O, were estimated as described in detail previously[20] using the relation $\tau_{C,eff}(D_2O) = \tau_{C,eff}(H_2O)D^t_{H_2O}/D^t_{D_2O}$, where $\tau_{C,eff}(H_2O)$ is derived from backbone amide ^{15}N relaxation data and D^t_j is the translational diffusion constant in solvent $j = D_2O$ or H_2O. Although the diffusion tensor for protein L is not isotropic ($D_{||}/D_\perp = 1.5$, where $D_{||}$ and $D_\perp$ are the components of the molecular diffusion tensor), we have previously found that, when the orientation of methyls is taken into account, the distribution of τ_C values is small (deviation of 8% from the isotropic value at the extreme case). Previous analyses, therefore, assumed an isotropic model for tumbling,[39,40] and we have done so here (10.2 ns in D_2O at 5 °C).

Following our previous work on MSG,[20] an axially symmetric diffusion tensor with $D_{||}/D_\perp = 1.21$ and with polar angles $\theta = 13°$ and $\phi = 48°$, describing the orientation of the unique diffusion axis relative to the molecular inertia coordinate frame, has been used in the analysis of the relaxation data reported here. Values of $\tau_{C,eff} = (2D_{||} + 4D_\perp)^{-1}$ of 56.0 and 41.4 ns were obtained for {U-[^{15}N,^2H], Ileδ1-[$^{13}CH_2D$]}-MSG and {U-[^{15}N,^2H], Ileδ1-[$^{13}CH_3$], Leu,Val-[$^{13}CH_3$,$^{12}CD_3$]}-labeled MSG, respectively, that reflect the difference in protein concentrations of the samples and the known solvent viscosity dependence on protein concentration.[20] Throughout this work we used the following expression for τ_C:[41]

$$\tau_C = \sum_{i=1}^{3} A_i \tau_i \qquad (1)$$

where $A_1 = (3/4)\sin^4(\alpha)$, $A_2 = 3\sin^2(\alpha)\cos^2(\alpha)$, $A_3 = [(3/2)\cos^2(\alpha) - 0.5]^2$, $\tau_1 = (4D_{||} + 2D_\perp)^{-1}$, $\tau_2 = (D_{||} + 5D_\perp)^{-1}$, and $\tau_3 = (6D_\perp)^{-1}$; α is the angle between the methyl three-fold axis (located along the $C^{\gamma 1}-C^{\delta 1}$ bond in Ile, along the $C^{\gamma}-C^{\delta 1}/C^{\gamma}-C^{\delta 2}$ bonds in Leu, and along the $C^{\beta}-C^{\gamma 1}/C^{\beta}-C^{\gamma 2}$ bonds in Val) and the unique principal axis of the diffusion tensor. Direction cosines for the appropriate three-fold axes were obtained from the X-ray coordinates of MSG,[31] PDB access code 1d8c. A value of $\tau_C = \tau_{C,eff}$ was used for those methyls that are not stereospecifically assigned or whose coordinates are not available in the X-ray structure.

Results and Discussion

(I) Measurement of S^2_{axis} Values from ^1H Relaxation in $^{13}CH_2D$ Methyl Groups. Theoretical Considerations. Figure 1a shows the energy level diagram for an isolated, rapidly rotating $^{13}CH_2D$ methyl group, neglecting contributions from the deuteron; only the triplet manifold ($I = 1$) is shown, which contains all of the ^1H transitions that give rise to proton signals. Each of the energy states is denoted by the product basis $|k\rangle|l\rangle$, where $|k\rangle$ and $|l\rangle$ are ^{13}C and ^1H eigenstates, respectively. In the case where the isolated methyl is attached to a protein tumbling in the macromolecular limit, such that $\omega_H\tau_C \gg 1$, where ω_H is the ^1H Larmor frequency, it can be shown that each of the ^1H single-quantum transitions (denoted by vertical lines) relaxes in a single-exponential manner with either fast ($R^F_{2,H}$, transitions shown in blue) or slow ($R^S_{2,H}$, red) rates. Thus, in the absence of ^{13}C decoupling and neglecting the very small scalar coupling involving the deuteron, a ^1H spectrum will consist of a "pair" of components separated by the one-bond $^1H-^{13}C$ scalar coupling constant, $^1J_{HC}$, with each component

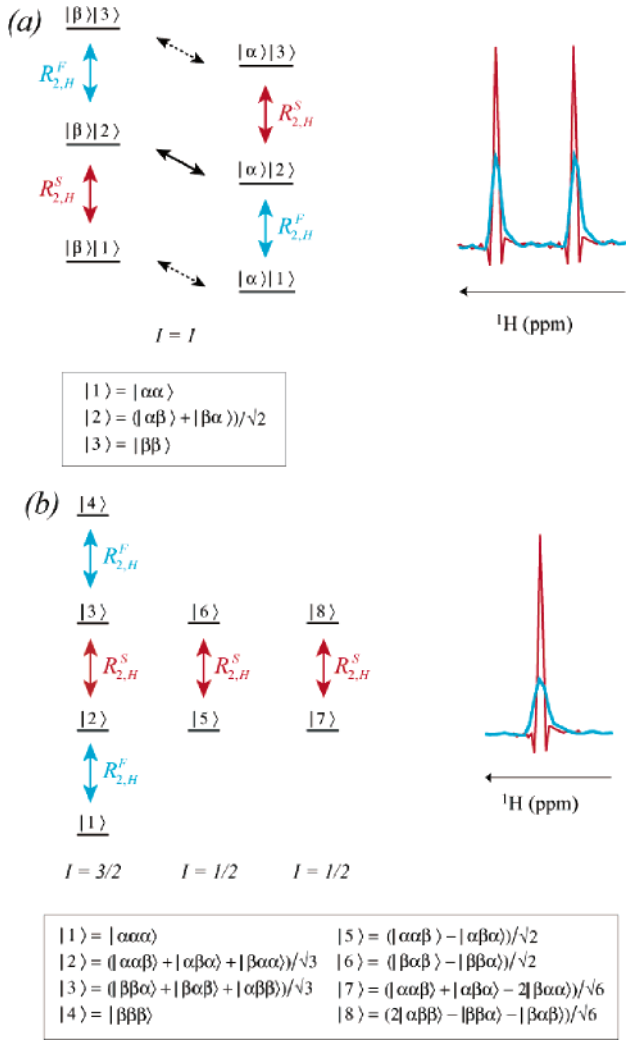

Figure 1. Energy level diagrams for (a) the $I = 1$ manifold of an AX_2 spin system, approximating a rapidly rotating $^{13}CH_2D$ methyl group where the ^2H spin is "silent", and (b) the X_3 spin system of a $(^{13}C)H_3$ methyl group. Slow (fast)-relaxing ^1H transitions are labeled $R^S_{2,H}$ ($R^F_{2,H}$) in both spin systems and are shown with red (blue) arrows, and slow (fast)-relaxing ^{13}C transitions in (a) are indicated by solid (dashed) black arrows. A product basis representation of each eigenfunction is used in (a), $|j\rangle|k\rangle$, where $j = \{\alpha,\beta\}$ is the ^{13}C spin state and $k = \{1,2,3\}$ is the wave function for a pair of magnetically equivalent ^1H spins. One-dimensional ^1H spectra obtained after a single-pulse excitation NMR experiment are shown on the right-hand side of each diagram, recorded without (a) and with (b) ^{13}C decoupling for $^{13}CH_2D$ and $^{13}CH_3$ methyl groups. Note that the doublet components in (a) are manipulated to produce spectra where each correlation ultimately is given by a singlet.[20,36]

in turn comprised of contributions from fast and slowly relaxing transitions. It can be shown that in the macromolecular limit described above and assuming very rapid rotation about the methyl three-fold axis,[20]

$$R^F_{2,H} - R^S_{2,H} \approx \frac{6}{5}P_2(\cos\theta_{axis,HH})P_2(\cos\theta_{axis,CH})\frac{S^2_{axis}\gamma_C\gamma_H^3\hbar^2\tau_C}{r^3_{CH}r^3_{HH}} \qquad (2)$$

where γ_k is the gyromagnetic ratio of spin k, r_{kl} is the distance between spins k and l, τ_C is the rotational correlation time (see eq 1), S_{axis} is the generalized order parameter of the methyl three-fold axis, $P_2(x) = (1/2)(3x^2 - 1)$, and $\theta_{axis,A}$ is the angle between

(39) Skrynnikov, N. R.; Millet, O.; Kay, L. E. *J. Am. Chem. Soc.* **2002**, *124*, 6449−6460.
(40) Tugarinov, V.; Kay, L. E. *J. Biomol. NMR* **2004**, *29*, 369−376.
(41) Wöessner, D. E. *J. Chem. Phys.* **1962**, *37*, 647−654.

the methyl symmetry axis and vector **A** that connects a pair of spins. In what follows, $\theta_{axis,HH} = 90°$, $\theta_{axis,CH} = 110.4°$, and $r_{CH} = 1.117$ Å have been used,[25,42] along with $r_{HH} = \sqrt{3} r_{CH} \sin\theta = 1.813$ Å that is in reasonable agreement with the value of 1.807 ± 0.012 Å reported for CH_3I based on $^1H-^1H$ and $^1H-^{13}C$ dipolar coupling ratios, $^1D_{HH}/^1D_{CH}$.[43]

Equation 2 is derived on the basis of infinitely fast methyl rotation. In addition, all spectral density terms evaluated at $\omega > 0$ have been ignored. Numerical simulations based on full expressions for $R^F_{2,H} - R^S_{2,H}$ (see Supporting Information) establish that, for the average set of motional parameters that is appropriate for Ileδ1 methyl groups of MSG ($\tau_C \approx 50$ ns, 37 °C; $S^2_{axis} = 0.6$; $\tau_f = 20$ ps), errors associated with the use of eq 2 are less than 0.3%. Errors do increase as S^2_{axis} decreases and for higher values of τ_f; however, they remain small for applications involving MSG (<2%), even for $S^2_{axis} = 0.1$ and $\tau_f = 20$ ps, with errors increasing to 4.5% for extreme cases where $S^2_{axis} = 0.1$, $\tau_f = 50$ ps. For smaller molecules, such as protein L ($\tau_C = 10$ ns at 5 °C), and for $S^2_{axis} = 0.5$ and $\tau_f = 20$ ps, errors are calculated to be close to 2% and to increase to approximately 5, 10, and 25% for ($S^2_{axis} = 0.5$, $\tau_f = 50$ ps), ($S^2_{axis} = 0.1$, $\tau_f = 20$ ps), and ($S^2_{axis} = 0.1$, $\tau_f = 50$ ps), respectively. It is clear that, for applications involving relatively small proteins and for methyl-containing side chains with large motions, there can be considerable error in extracted values of S^2_{axis} using eq 2. Nevertheless, for the majority of methyl-containing residues in proteins with $\tau_C > 10$ ns, and especially for much larger systems, systematic errors in ^1H-derived S^2_{axis} values are more sensitive to possible variations in local methyl geometry than to the approximate nature of eq 2. For example, although $R^F_{2,H} - R^S_{2,H}$ is insensitive to small deviations in $\theta_{axis,HH}$ ($\sim 1-2°$), it is more sensitive to changes in $\theta_{axis,CH}$, where a 1° change corresponds to a 5% deviation in the difference. Fortunately, values of $P_2(\cos\theta_{axis,CH})/r^3_{CH}$ are well known, at least on average, from dipolar coupling-based studies of weakly aligned proteins.[35,42] A discussion of the effects of variability of methyl geometry on the extracted values of S^2_{axis} has appeared previously.[44]

An additional approximation in eq 2 is that it is derived for the limiting case of an isolated methyl group, where relaxation contributions from external protons are by definition zero. As discussed in the Introduction, relaxation contributions to individual transitions from external protons can be non-negligible. For example, for dynamics parameters of $\tau_C = 56$ ns, $S^2_{axis} = 0.6$, and $\tau_f = 20$ ps (corresponding to average values for Ile residues in the $^{13}CH_2D$ methyl-labeled MSG sample), external protons contribute only approximately 0.3 (2)% to net $R^F_{2,H}$ ($R^S_{2,H}$) rates when $r_{eff} = (\sum_{ext}(1/r^6_{HHext}))^{-1/6} = 5.5$ Å (where r_{HHext} is the distance between the methyl protons of the $^{13}CH_2D$ group and a proton external to the methyl of interest). However, external protons contribute 4 (20) and 30 (70)% when r_{eff} decreases to 3.5 and 2.4 Å, respectively. In the case of {U-[^{15}N,^2H], Ileδ1-[$^{13}CH_2D$]}-labeled MSG considered here, where the average r_{eff} value is 5.5 Å, external protons make small contributions even to the relaxation of the individual transitions, in general, but for Ileδ1, Leu,Val-[$^{13}CH_2D$]-labeled samples the situation will be quite different. By contrast, by taking the difference $R^F_{2,H} - R^S_{2,H}$, contributions to ^1H relaxation from dipolar interactions with external spins are subtracted to first order, as well as possible contributions due to chemical exchange.

The contribution to the decay of slow and fast-relaxing ^1H coherences in $^{13}CH_2D$ methyl groups from external proton spins can be evaluated using the formalism of Abragam, describing the evolution of the density matrix due to spin relaxation.[24] We obtain

$$\frac{d}{dt}\begin{bmatrix} L_1 \\ L_2 \end{bmatrix} = -k_{HH}\begin{bmatrix} 7 & -2 \\ -2 & 7 \end{bmatrix}\begin{bmatrix} L_1 \\ L_2 \end{bmatrix} \quad (3)$$

where L_1 and L_2 are the intensities of the time-dependent transverse magnetization components that derive from the elements $|\beta\rangle|2\rangle\langle\beta|\langle 3| + |\alpha\rangle|1\rangle\langle\alpha|\langle 2|$ and $|\beta\rangle|1\rangle\langle\beta|\langle 2| + |\alpha\rangle|2\rangle\langle\alpha|\langle 3|$, respectively (see Figure 1a). In eq 3, $k_{HH} = \sum_{ext}(1/20)(\hbar^2 \gamma_H{}^4 \tau_C/r^6_{HHext})$, with all symbols defined as above. Here, the order parameter for each methyl−external spin interaction is assumed to be equal to 1, so that an upper estimate of the contributions from external spins is obtained. It is clear from eq 3 that cross-relaxation leads to a coupling of the "slow" and "fast" components of the signal. However, simulations that assume that k_{HH} can be approximated by considering only a single proton with an effective external proton−methyl distance, $(\sum_{ext}(1/r^6_{HHext}))^{-1/6} = 2$ Å, show that for {Ileδ1-[$^{13}CH_2D$]}-labeled MSG the errors in $R^F_{2,H} - R^S_{2,H}$ are below 2% and are effectively zero beyond a distance of ~3 Å. In the case of {Ileδ1-[$^{13}CH_2D$]}- and {Ileδ1-[$^{13}CH_2D$], Val,Leu-[$^{13}CH_2D$, $^{13}CH_2D$]}-labeled MSG, where average distances of 5.9 and 2.9 Å (minimum distances of 2.5 and 1.9 Å) are calculated, these effects can be safely neglected.

The above discussion makes it clear that, in order to measure accurate values of S^2_{axis}, it is first necessary to separate lines derived from fast and slowly relaxing transitions so that their relaxation rates can be determined independently. In what follows below, such a scheme is presented.

Separation of "Slow" and "Fast" Relaxing ^1H Transitions in $^{13}CH_2D$ Methyl Groups. Figure 2a shows the pulse scheme that has been derived for the measurement of $R^S_{2,H}$ and $R^F_{2,H}$ relaxation rates in $^{13}CH_2D$ methyl groups in proteins. The sequence follows directly from a $^{13}CH_2D$-TROSY experiment developed earlier for ^2H relaxation measurements in high-molecular-weight proteins[20] and from a relaxation-optimized scheme that has been employed to measure ^1H,^{13}C correlations in $^{13}CH_2D$ methyls.[36] The interested reader is referred to the literature for a detailed description of the mechanics of the experiment; here, only that portion of the sequence that is unique to the present work is described in any detail.

Our goal in what follows is to derive an expression for the magnetization at the start of the t_2 acquisition period, $M(t_1{=}0; t_2{=}0)$, that will clarify how relaxation rates of individual coherences can be extracted. Briefly, the elements between points *a* and *b* in Figure 2a ensure that only the slowly relaxing ^{13}C transition ($C_{Y,slow} = C_Y|2\rangle\langle 2|$, where C_k is the *k* component of C magnetization; solid horizontal line of Figure 1a) evolves during the t_1 period, to produce terms of the form $C_Y|2\rangle\langle 2|\cos(\Omega_C t_1) - C_X|2\rangle\langle 2|\sin(\Omega_C t_1)$ at point *c*. In what follows, consider first the case where $\phi 5 = \phi 6 = -x$ and where the dashed ^{13}C 180° pulse at the end of the scheme is omitted.

(42) Ottiger, M.; Bax, A. *J. Am. Chem. Soc.* **1999**, *121*, 4690−4695.
(43) Wooten, J. B.; Savitsky, G. B.; Jacobus, J.; Beyerlein, A. L.; Emsley, J. W. *J. Chem. Phys.* **1979**, *70*, 438−442.
(44) Nicholson, L. K.; Kay, L. E.; Baldisseri, D. M.; Arango, J.; Young, P. E.; Bax, A.; Torchia, D. A. *Biochemistry* **1992**, *31*, 5253−5263.

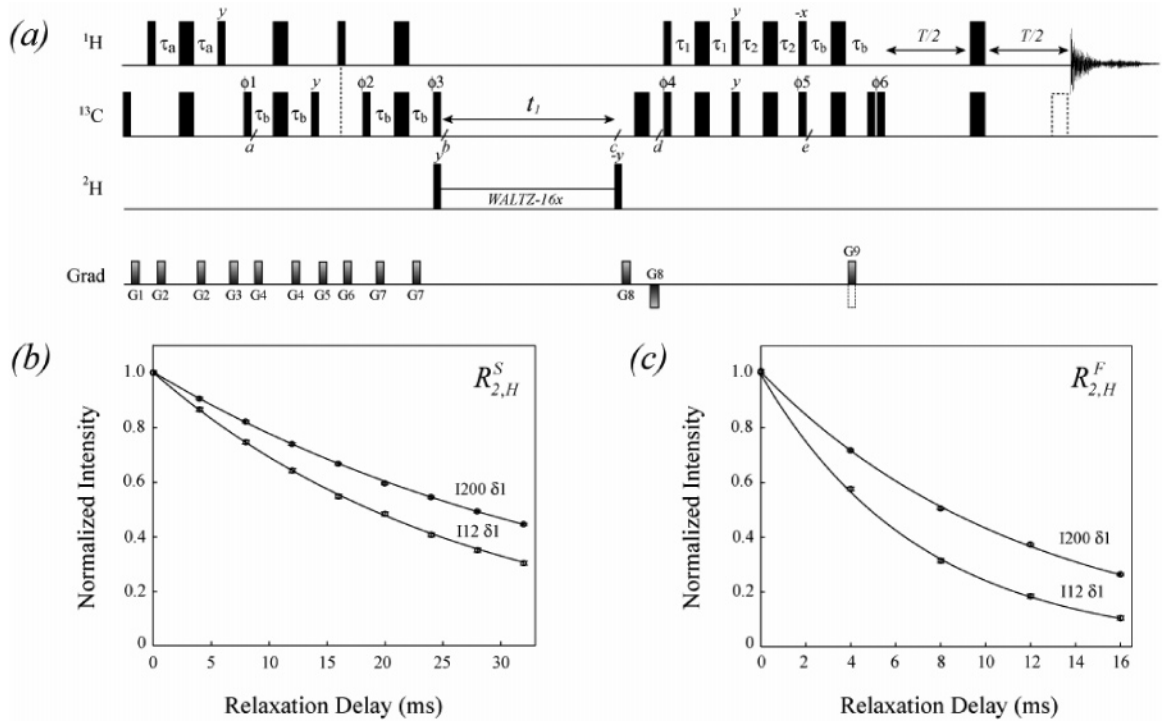

Figure 2. (a) TROSY-based pulse scheme for the measurement of $R^S_{2,H}$ and $R^F_{2,H}$ ^{1}H relaxation rates in $^{13}CH_2D$ methyl groups of highly deuterated proteins. All narrow (wide) rectangular pulses are applied with flip angles of 90 (180)° along the *x*-axis unless indicated otherwise. The ^{1}H, ^{2}H, and ^{13}C carrier frequencies are positioned in the center of the Ileδ1 methyl region at 1, 1, and 12 ppm, respectively. All ^{1}H and ^{13}C pulses are applied with the highest possible power, while a 1.7 kHz field is used for ^{2}H pulses and 0.7 kHz for ^{2}H decoupling. Delays are as follows: $\tau_a = 1.8$ ms; $\tau_b = 1$ ms; $2\tau_1 = 1.33$ ms; $2\tau_2 = 1.57$ ms; T is a variable relaxation delay. The durations and strengths of the *z*-gradients in units of ms and G/cm, respectively, are as follow: G1 = 1, 7.5; G2 = 0.5, 10; G3 = 1, −8; G4 = 0.1, 2; G5 = 0.5, 12; G6 = 0.3, 12; G7 = 0.3, −5; G8 = 0.25, 30; and G9 = 0.125, 30). The phase cycle is as follows: $\phi1 = x,-x$; $\phi2 = 2(x),2(-x)$; $\phi3 = 4(y),4(-y)$; $\phi4 = x$; $\phi5 = -x$; $\phi6 = -x$ ($R^S_{2,H}$) or x ($R^F_{2,H}$); rec. $= x,-x,-x,x$. The 180° ^{13}C pulse, shown with a dashed line, is included only when $R^F_{2,H}$ is measured. Quadrature detection in F_1 is achieved via a gradient-enhanced sensitivity scheme,[45,46] where for each t_1 value a pair of spectra are recorded with $\phi4 = x$,G9 and $\phi4 = -x$,−G9. Splittings in the ^{1}H dimension resulting from the one-bond ^{1}H−^{13}C scalar coupling are removed by recording a pair of data sets with (i) $\phi5 = -x$, $\phi6 = -x(x)$ for $R^S_{2,H}$ ($R^F_{2,H}$) measurements and (ii) $\phi5$,$\phi6$ simultaneously inverted, and by a postacquisition processing procedure described in detail previously[20] that involves taking appropriate linear combinations of the data (see, for example, Figure 3 of ref 20). (b,c) Exponential decay curves that quantify $R^S_{2,H}$ (b) and $R^F_{2,H}$ (c) for Ile12 and Ile200 of {U-[^{15}N,^{2}H], Ileδ1-[$^{13}CH_2D$]}-MSG (37 °C), after processing as described in the text.

For simplicity, the effects of coherence transfer gradients G8 and G9 are not included in the discussion. The element between d and e transforms magnetization from the slowly relaxing ^{13}C components to the slowly relaxing ^{1}H lines,[20,36,47] $C_{Y,slow} \rightarrow 2C_ZH_{Y,slow}$, $C_{X,slow} \rightarrow 2C_ZH_{X,slow}$. Each of the terms $C_{j,slow}$ and $2C_ZH_{j,slow}$, j = X, Y, can be defined in terms of individual transitions,[36] but this is not necessary presently. We consider here the fate of $2C_ZH_{Y,slow}$, which corresponds to the relevant term at $t_1 = 0$, noting that a similar transfer pathway pertains to $2C_ZH_{X,slow}$. During the subsequent delay of $2\tau_b = 1/(4^1J_{HC})$, $2C_ZH_{Y,slow}$ evolves to $1/\sqrt{2}\{2C_ZH_{Y,slow} - H_{X,slow}\} = AP_{Y,slow} - IP_{X,slow}$, with $AP_{Y,slow} = \sqrt{2}C_ZH_{Y,slow}$ and $IP_{X,slow} = 1/\sqrt{2}H_{X,slow}$. Subsequently, during the following relaxation delay of duration T, $AP_{Y,slow} - IP_{X,slow}$ evolves so that the magnetization at the start of t_2 is given by $M_1(t_1{=}0;\ t_2{=}0) = \exp(-R^S_{2,H}T)\{AP_{Y,slow}\cos(\theta) - IP_{X,slow}\sin(\theta) - IP_{X,slow}\cos(\theta) - AP_{Y,slow}\sin(\theta)\}$, with $\theta = \pi^1J_{HC}T$, and where relaxation during other intervals of the pulse scheme is ignored. A second experiment is recorded with $\phi5 = \phi6 = x$, and again with the dashed ^{13}C 180° pulse at the end of the scheme omitted. In this case, $M_2(t_1{=}0;\ t_2{=}0) = \exp(-R^S_{2,H}T)\{AP_{Y,slow}\cos(\theta) - IP_{X,slow}\sin(\theta) + IP_{X,slow}\cos(\theta) + AP_{Y,slow}\sin(\theta)\}$. Addition (subtraction) of the pair of data sets derived from M_1 and M_2 gives new data matrices, with $M_{add}(t_1{=}0;\ t_2{=}0) = 2\exp(-R^S_{2,H}T)\{AP_{Y,slow}\cos(\theta) - IP_{X,slow}\sin(\theta)\}$ and $M_{subtract}(t_1{=}0;\ t_2{=}0) = 2\exp(-R^S_{2,H}T)\{IP_{X,slow}\cos(\theta) + AP_{Y,slow}\sin(\theta)\}$. Values of T that are multiples of $1/(2^1J_{HC})$ are chosen so that for even multiples $\theta = \pi k$, where k is an integer (i.e., $T = 0,\ 1/^1J_{HC},\ 2/^1J_{HC}$, ...), and the addition/subtraction spectra have the form $(-1)^k\exp(-R^S_{2,H}T)AP_{Y,slow}$ and $(-1)^k\exp(-R^S_{2,H}T)IP_{X,slow}$, respectively. These data sets can be subsequently manipulated exactly as described in detail previously,[20,36] to produce spectra with pure absorption line shapes, with only a single peak for each correlation. Each second data set is multiplied by −1 (i.e., $T = 1/^1J_{HC},\ 3/^1J_{HC}$, ...) so that intensities in all spectra are positive; thus, each correlation decays with a time dependence given by $\exp(-R^S_{2,H}T)$. In a similar manner, when an odd multiple of $1/(2^1J_{HC})$ is chosen so that $\theta = (2k + 1)\pi/2$, the addition/subtraction spectra have the form $-(-1)^k\exp(-R^S_{2,H}T)IP_{X,slow}$ and $(-1)^k\exp(-R^S_{2,H}T)AP_{Y,slow}$, respectively. These spectra can be suitably manipulated to produce data sets with absorptive lines that decay as $\exp(-R^S_{2,H}T)$, as well. Finally, data from both even and odd multiples of $1/(2^1J_{HC})$ are combined, as in

(45) Kay, L. E.; Keifer, P.; Saarinen, T. *J. Am. Chem. Soc.* **1992**, *114*, 10663−10665.
(46) Schleucher, J.; Sattler, M.; Griesinger, C. *Angew. Chem., Int. Ed. Engl.* **1993**, *32*, 1489−1491.
(47) Mádi, Z. L.; Brutscher, B.; Schülte-Hebrüggen, T.; Brüschweiler, R.; Ernst, R. R. *Chem. Phys. Lett.* **1997**, *268*, 300−305.

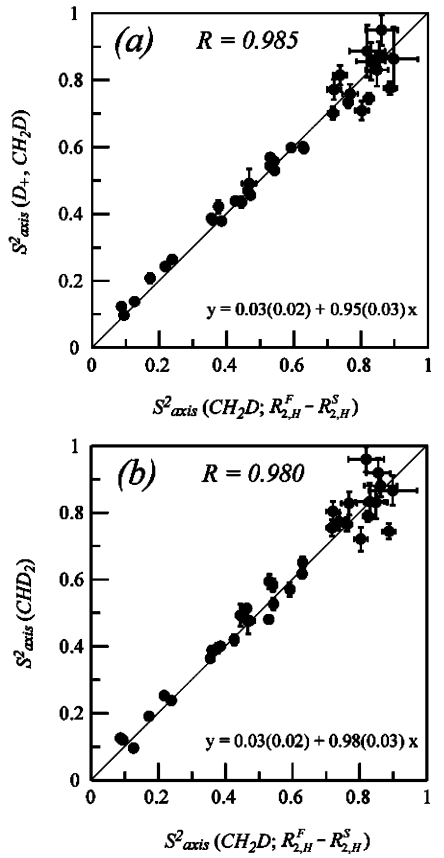

Figure 3. Linear correlation plots of (a) $R(D_+,{}^{13}CH_2D)$-derived S^2_{axis}[20] and (b) $R({}^{13}CHD_2)$-derived S^2_{axis}[20] of Ile residues of MSG (*y*-axis) vs S^2_{axis} values obtained in this work from $R^F_{2,H} - R^S_{2,H}$ measured on $^{13}CH_2D$ methyl groups of MSG (*x*-axis). See text for the methyl geometry parameters used to obtain ^1H relaxation-derived S^2_{axis} values. Pearson linear correlation coefficients (R) are indicated at the top of each plot, along with the equation for the best-fit line at the bottom. The correlation $y = x$ is drawn in solid black.

Figure 2b, and subsequently fit to extract $R^S_{2,H}$. In a manner similar to that described above, values of $R^F_{2,H}$ are obtained (Figure 2c) by recording spectra where phase $\phi 6$ is inverted and the final ^{13}C 180° pulse (dashed) is included. Inversion of $\phi 6$ ensures that only the fast decaying signal is monitored during T, while insertion of the 180° carbon pulse converts fast to slowly relaxing magnetization for detection during t_2. It is noteworthy that absorptive line shapes in F_2 are obtained only in the case where $T = k/(2^1J_{HC})$; for Ileδ1 groups studied here, $^1J_{CH}$ values are very homogeneous (125.1 ± 0.4 Hz in $^{13}CH_2D$ isotopomers[35]), and no dispersive components were observed in the experiments.

Experimental Verification. Figure 2b,c shows magnetization decay curves for Ile12 and Ile200, measured in a highly deuterated, {U-[^{15}N,^2H], Ileδ1-[$^{13}CH_2D$]}-MSG sample. Average $R^F_{2,H}$ and $R^S_{2,H}$ rates of 141 ± 65 and 38 ± 15 s^{-1} were obtained, based on the quantification of 36 residues. S^2_{axis} values obtained from experimentally derived differences, $R^F_{2,H} - R^S_{2,H}$, were calculated using eq 2, along with methyl geometry parameters specified above. These were subsequently compared with S^2_{axis} values obtained from our previous ^2H relaxation studies[20] where either $^{13}CH_2D$ or $^{13}CHD_2$ probes of motion were used (Figure 3a,b). It is readily apparent that S^2_{axis} values are highly correlated in both cases, with the correlation well approximated by the line $y = x$, providing good evidence for the absence of significant systematic errors in ^1H-derived order parameters, as expected from simulations (see above).

The experiment of Figure 2a is on average a factor of 2 more sensitive than the corresponding $^{13}CH_2D$-TROSY-based scheme that measures the relaxation of deuterium transverse magnetization.[20] This value is in good agreement with the estimated losses that are associated with magnetization transfer steps to and from ^2H nuclei in the pulse schemes for ^2H relaxation measurements.

(II) Measurement of S^2_{axis} Values from ^1H Relaxation in $^{13}CH_3$ Methyl Groups. Theoretical Considerations. The energy level diagram for an isolated, rapidly rotating methyl group ($[^{13}C]H_3$) is shown in Figure 1b, where for simplicity the ^{13}C spin state is neglected, since the focus here is on relaxation of ^1H single-quantum coherences. As described in detail previously,[48] in the limit of a rapidly rotating isolated methyl group attached to a macromolecule, each of the proton single-quantum transitions (denoted by vertical arrows in Figure 1b) relaxes exponentially. It is straightforward to show that, under these conditions, the relaxation of a pair of transitions occurs rapidly, with a rate $R^F_{2,H}$, while the remaining lines relax slowly with a rate $R^S_{2,H}$, and that

$$R^F_{2,H} - R^S_{2,H} \approx \frac{9}{5}[P_2(\cos\theta_{axis,HH})]^2 \frac{S^2_{axis}\gamma_H^4\hbar^2\tau_C}{r_{HH}^6} \quad (4)$$

where all symbols are as defined above.

More complex equations that are valid in general can be derived and are provided in the Supporting Information. Simulations that include the complete expressions for the relaxation of protons in an isolated $^{13}CH_3$ group, using typical dynamics parameters obtained for {U-[^{15}N,^2H], Ile-[$^{13}CH_3$], Leu,Val-[$^{13}CH_3$,$^{13}CD_3$]}-labeled MSG (τ_C = 42 ns; S^2_{axis} = 0.6; τ_f = 50 ps), show that the errors obtained when using eq 4 are small (on the order of 0.2%) and remain low (0.5%) even for (S^2_{axis} = 0.1; τ_f = 50 ps). In the case of protein L (τ_C = 10.2 ns; S^2_{axis} = 0.5; τ_f = 50 ps), errors are on the order of 1% and increase to 2.5% for S^2_{axis} = 0.2, the lowest value observed among Ile(δ1), Leu, and Val methyls in this protein.

As in the case of studies of dynamics involving $^{13}CH_2D$ groups discussed above, contributions from external protons remain a potential concern in applications involving ^1H spin relaxation in $^{13}CH_3$ groups. The evolution of slow and fast-relaxing ^1H coherences in $^{13}CH_3$ methyl groups due to interactions with external protons can be modeled by

$$\frac{d}{dt}\begin{bmatrix} L_1 - L_3 \\ L_2 \\ L_1 + L_3 \\ L_4 \end{bmatrix} = -k_{HH}\begin{bmatrix} 9 & 0 & 0 & 0 \\ 0 & 9 & -4 & 2\sqrt{2} \\ 0 & -4 & 9 & -2\sqrt{2} \\ 0 & 2\sqrt{2} & -2\sqrt{2} & 7 \end{bmatrix}\begin{bmatrix} L_1 - L_3 \\ L_2 \\ L_1 + L_3 \\ L_4 \end{bmatrix} \quad (5)$$

where the variables L_i are the intensities of the time-dependent transverse magnetization components associated with the transitions listed in Figure 1b,

(48) Tugarinov, V.; Hwang, P. M.; Ollerenshaw, J. E.; Kay, L. E. *J. Am. Chem. Soc.* **2003**, *125*, 10420−10428.

$$L_1 - L_3 \leftrightarrow \sum_{i\neq j\neq k} H_+{}^i(|\beta\beta\rangle^{j,k}\langle\beta\beta|^{j,k} - |\alpha\alpha\rangle^{j,k}\langle\alpha\alpha|^{j,k}) = \sqrt{3}(|3\rangle\langle 4| - |1\rangle\langle 2|)$$

$$L_1 + L_3 \leftrightarrow \sum_{i\neq j\neq k} H_+{}^i(|\beta\beta\rangle^{j,k}\langle\beta\beta|^{j,k} + |\alpha\alpha\rangle^{j,k}\langle\alpha\alpha|^{j,k}) = \sqrt{3}(|3\rangle\langle 4| + |1\rangle\langle 2|) \quad (6)$$

$$L_2 \leftrightarrow \sum_{i\neq j\neq k} H_+{}^i(|\alpha\beta\rangle^{j,k}\langle\alpha\beta|^{j,k} + |\beta\alpha\rangle^{j,k}\langle\beta\alpha|^{j,k}) = (2|2\rangle\langle 3| + |5\rangle\langle 6| + |7\rangle\langle 8|)$$

$$L_4 \leftrightarrow \sum_{i\neq j\neq k} \frac{1}{\sqrt{2}} H_+{}^i(|\alpha\beta\rangle^{j,k}\langle\beta\alpha|^{j,k} + |\beta\alpha\rangle^{j,k}\langle\alpha\beta|^{j,k}) = \sqrt{2}(|2\rangle\langle 3| - |5\rangle\langle 6| - |7\rangle\langle 8|)$$

Equation 6 is derived following the approach detailed by Abragam.[24] Here, $H_+ = H_X + iH_Y$ (or alternatively $H_+ = |\alpha\rangle\langle\beta|$), with indices $i, j, k = 1, 2, 3$ ($i \neq j \neq k$) distinguishing the three ^{1}H spins, and k_{HH} (eq 5) is defined in eq 3 above. Simulations can be performed that take into account the initial conditions of magnetization at the start of the relaxation period. As we describe in the next section, $R^F_{2,H} - R^S_{2,H}$ values have been obtained using two different experiments to measure $R^F_{2,H}$, and in both cases simulations based on eqs 5 and 6 predict errors in $R^F_{2,H} - R^S_{2,H}$ on the order of 2% or less for $\sum_{ext}(1/r^6_{HHext})^{-1/6} \geq 2.5$ Å. In this regard, it is of interest to note that average values of $\sum_{ext}(1/r^6_{HHext})^{-1/6}$ calculated from the X-ray coordinates of {U-[^{15}N,^{2}H], Ileδ1-[$^{13}CH_3$], Leu,Val-[$^{13}CH_3$, $^{12}CD_3$]}-labeled samples of protein L[30] and MSG[31] dissolved in D_2O are 3.5 Å, with the shortest values for protein L and MSG being 2.6 and 2.0 Å, respectively. Thus, errors in ^{1}H-derived S^2_{axis} values ($^{13}CH_3$ methyls) from spin-flips are expected to be below contributions from noise for most residues in highly deuterated proteins (see below).

Pulse Schemes for Measurement of $R^S_{2,H}$ and $R^F_{2,H}$ in $^{13}CH_3$ Methyl Groups. Figure 4a shows the pulse scheme that has been used to measure $R^S_{2,H}$ in ^{13}C-labeled methyl groups. The pulse sequence is essentially an HMQC experiment,[49,50] with an element that selects for slowly relaxing ^{1}H−^{13}C double/zero quantum transitions[33] during the interval between points *a* and *b*, where $2\tau_b = 1/(4^1J_{HC})$. These slowly relaxing coherences are subsequently converted exclusively to slowly relaxing proton lines (red vertical arrows in Figure 1b) by the application of the ^{13}C 90° pulse of phase ϕ3, as has been described in detail previously.[33] Thus, at the start of the *T* period, $L_1 - L_3 = L_1 + L_3 = L_4 = 0$, $L_2 \neq 0$ (see eqs 5 and 6). Subsequently, the slowly relaxing proton magnetization is allowed to decay for duration *T*, with ^{1}H−^{13}C dipolar/^{1}H CSA cross-correlated spin relaxation contributions eliminated by the ^{13}C 180° pulses applied during the course of the *T* period. As in standard heteronuclear relaxation experiments, a series of two-dimensional ^{1}H−^{13}C correlation maps are recorded, and $R^S_{2,H}$ is quantified from the exponential decay of magnetization.

The pulse schemes used for the measurement of $R^F_{2,H}$ are shown in Figure 4b. The two sequences are very similar, with the main distinction arising from the difference in the initial magnetization conditions at the start of the relaxation period of duration *T*. Measurement of relaxation rates with both schemes provides an opportunity to establish the robustness of the methodology and to evaluate the effects of initial conditions on the extracted rate constants. In the first scheme, denoted by $R(L_1 + L_3)$, slowly relaxing ^{1}H−^{13}C double/zero quantum coherences are evolved during t_1, as in the experiment of Figure 4a. The ^{1}H 90° pulse at point *a* converts a fraction of these slowly relaxing coherences to rapidly relaxing ones, and these rapidly relaxing elements are selected by the interval between points *a* and *b* ($2\tau_b = 1/(4^1J_{HC})$). Thus, immediately after the ^{13}C 90° pulse of phase ϕ5, the coherences of interest are $C_X[|1\rangle\langle 2| + |2\rangle\langle 1| - |3\rangle\langle 4| - |4\rangle\langle 3|]$, which subsequently evolve to $C_Y[|1\rangle\langle 2| + |2\rangle\langle 1| + |3\rangle\langle 4| + |4\rangle\langle 3|]$ during the second element of duration $2\tau_b$, between points *b* and *c*. Application of the ^{13}C 90° ϕ6 pulse converts ^{1}H−^{13}C multiple-quantum coherence to ^{1}H single-quantum magnetization (the sum of the transitions indicated in blue in Figure 1b), which relaxes with a time constant $R^F_{2,H}$ during the delay *T*, with cross-correlated spin relaxation interactions refocused by the central ^{1}H 180° pulse (^{1}H−^{13}C dipolar/^{1}H−^{1}H dipolar, ^{1}H−^{1}H dipolar/^{1}H CSA) or by the ^{13}C 180° pulses (^{1}H−^{13}C dipolar/^{1}H−^{1}H dipolar, ^{1}H−^{13}C dipolar/^{1}H CSA). The ^{1}H 90° pulse that follows converts a portion of the fast-decaying ^{1}H magnetization to slowly relaxing signal that significantly improves spectral resolution in t_2 as well as the sensitivity of the resultant data set. In the second scheme, the relaxation of ^{1}H single-quantum magnetization corresponding to the difference of the transitions indicated in blue in Figure 1b occurs during *T*, with the element between *d* and *e* converting magnetization to in-phase for detection during t_2. Detailed calculations show that in the macromolecular limit and neglecting contributions to relaxation from external ^{1}H spins, rates measured via either scheme should be identical.

There are differences in the two schemes for measuring $R^F_{2,H}$, however, that derive from changes in the initial conditions of magnetization at the start of the relaxation period, *T*. In the case of scheme 1 (denoted by $R(L_1 + L_3)$ in Figure 4), $L_1 - L_3 = L_2 = L_4 = 0$, $L_1 + L_3 \neq 0$, and according to the relaxation model of eq 5 the contributions from external protons can lead to nonexponential relaxation; however, because only one mode is populated initially, nonexponential effects are small. In the case of scheme 2 ($R(L_1 - L_3)$), $L_1 - L_3 \neq 0$, $L_1 + L_3 = L_2 = L_4 = 0$, and external protons simply elevate the decay, which remains single exponential. It is noteworthy that the decays of modes $\{L_2\}$ and $\{L_1 + L_3\}$ are coupled, and that analogous equations describe their decay, while the decays of $\{L_2\}$ and $\{L_1 - L_3\}$ are not coupled, eq 5. Qualitatively we might expect, therefore, that the contributions from external spins might "subtract out" better in experiments that measure $R^F_{2,H} - R^S_{2,H}$ values on the basis of the decay of $\{L_2\}$ and $\{L_1 + L_3\}$ than if the decay rates of $\{L_2\}$ and $\{L_1 - L_3\}$ are measured. This is observed in computations for very short distances ($(\sum_{ext}(1/r^6_{HHext}))^{-1/6} = 2.0$ Å, where errors on the order of 2 and 15% are calculated for $R^F_{2,H} - R^S_{2,H}$ values based on $R^F_{2,H}$ rates obtained from the decay of $\{L_1 + L_3\}$ and $\{L_1 - L_3\}$, respectively. It must be emphasized that the calculations were performed assuming that the order parameter for the external proton−methyl interaction is 1, and thus the errors estimated are very much upper bounds. Although scheme 1, which measures the decay of $\{L_1 + L_3\}$,

(49) Mueller, L. *J. Am. Chem. Soc.* **1979**, *101*, 4481−4484.
(50) Bax, A.; Griffey, R. H.; Hawkings, B. L. *J. Magn. Reson.* **1983**, *55*, 301−315.

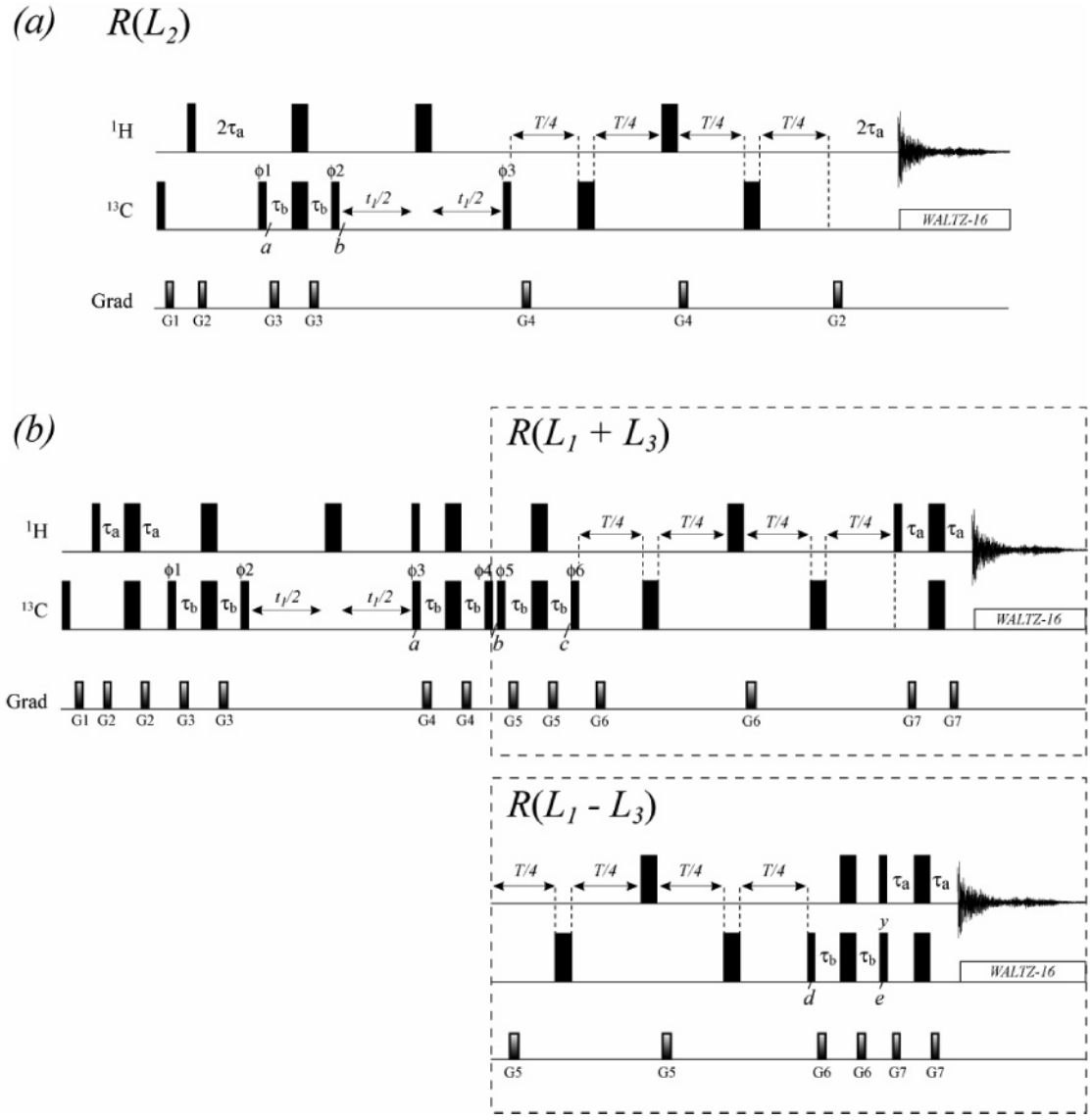

Figure 4. Pulse schemes for the measurement of (a) $R^{S}_{2,H}$ and (b) $R^{F}_{2,H}$ relaxation rates in $^{13}CH_3$ methyl groups. Two sequences are illustrated for measuring $R^{F}_{2,H}$ rates that differ in the initial magnetization conditions at the start of the T period, as described in the text. Many of the details of the implementation are as described in the legend to Figure 2. ^{13}C WALTZ-16 decoupling[51] is achieved using a 2-kHz field. Delays are as follows: $\tau_a = 1.8$ ms; $\tau_b = 1$ ms; T is a variable relaxation delay. The durations and strengths of z-gradients in units of ms and G/cm are as follow: in scheme (a), G1 = 1, 30; G2 = 0.5, 10; G3 = 0.3, −20; and G4 = 0.075, −30; in scheme (b) for $L_1 + L_3$, G1 = 1, 30; G2 = 0.5, 10; G3 = 0.3, −20; G4 = 0.4, 12; G5 = 0.25, 5; G6 = 0.05, −9; G7 = 0.5, −7; and in scheme (b) for $L_1 - L_3$, G1 = 1, 30; G2 = 0.5, 10; G3 = 0.3, −20; G4 = 0.4, 12; G5 = 0.05, −9; G6 = 0.25, 5; G7 = 0.5, −7. The phase cycle is as follows: for scheme (a), $\phi1 = x,-x$; $\phi2 = 2(y),2(-y)$; $\phi3 = x$; rec. $= x,-x$; and for both schemes (b), $\phi1 = x,-x$; $\phi2 = 2(y),2(-y)$; $\phi3 = 4(y),4(-y)$; $\phi4 = 8(y),8(-y)$; $\phi5 = y$; $\phi6 = x$; rec. $= 4(x,-x),4(-x,x)$. Quadrature detection in F_1 is achieved by STATES incrementation[52] of $\phi3$ (scheme a) and of $\phi3$, $\phi4$ (scheme b, $L_1 + L_3$ or $L_1 - L_3$).

is thus preferred (with errors less than 2% for any calculated r_{eff} difference), experimentally we have observed little difference in the quality of the extracted dynamics parameters from either approach, as described in the subsequent section. Finally, we wish to emphasize that the initial magnetization conditions are important to consider in the experimental design. In all of the schemes described here, only the magnetization mode whose relaxation is to be measured is populated at $T = 0$. This minimizes nonexponential relaxation behavior that, at least in some cases, would certainly exist and leads to far better subtraction of contributions from external proton spins.

Experimental Verification. The pulse schemes of Figure 4 have been applied to a pair of proteins including {U-[^{15}N,^{2}H], Ileδ1-[$^{13}CH_3$], Leu,Val-[$^{13}CH_3$,$^{12}CD_3$]}-protein L (5 °C) and {U-[^{15}N,^{2}H], Ileδ1-[$^{13}CH_3$],Leu, Val-[$^{13}CH_3$,$^{12}CD_3$]}-MSG (37 °C). Average $R^{F}_{2,H}$ ($R^{S}_{2,H}$) rates of 54 ± 17 (8 ± 2) and 211 ± 82 (26 ± 9) s^{-1} were obtained for the two samples listed above (± refers to one standard deviation). The large differences in rates, as expected, provides a measure of confidence that $R^{F}_{2,H} - R^{S}_{2,H}$ can be quantified with small errors and that accurate values of S^2_{axis} can be extracted. Figure 5a,b illustrates decay curves for a pair of correlations from Leu 128(δ1) and Val 535(γ2) in {U-[^{15}N,^{2}H], Ileδ1-[$^{13}CH_3$], Leu,Val-[$^{13}CH_3$,$^{12}CD_3$]}-MSG, along with single-exponential fits of the data, from which ^{1}H relaxation rates were obtained. The corresponding decay curves for a pair of cross-peaks from protein L (Ile58 δ1 and Leu38 δ2) are shown in the insets.

Figure 5c−f shows linear correlation plots of ^{2}H-derived S^2_{axis} (y-axis) *vs* S^2_{axis} obtained from $R^{F}_{2,H} - R^{S}_{2,H}$ using eq 4 (x-axis) for {U-[^{15}N,^{2}H], Ileδ1-[$^{13}CH_3$], Leu,Val-[$^{13}CH_3$,$^{12}CD_3$]}-

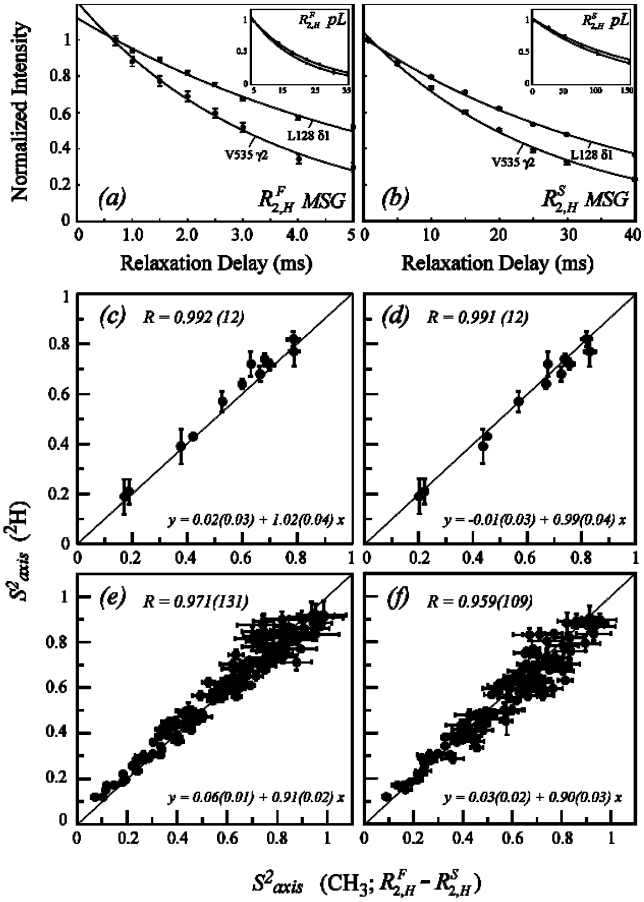

Figure 5. (a,b) Exponential decay curves quantifying $R^F_{2,H}$ (a) and $R^S_{2,H}$ (b) for Val 535(γ2) and Leu 128(δ1) of {U-[^{15}N,^{2}H], Ileδ1-[^{13}CH$_3$], Leu,Val-[^{13}CH$_3$,^{13}CD$_3$]}-labeled MSG and Ile 58(δ1), Leu 38(δ2) of {U-[^{15}N,^{2}H], Ileδ1-[^{13}CH$_3$], Leu,Val-[^{13}CH$_3$,^{13}CD$_3$]}-labeled protein L (insets). (c,d) Linear correlation plots of ^{2}H-derived S^2_{axis} values of Ile(δ1), Leu, and Val methyl groups in protein L[39] vs S^2_{axis} values calculated from $R^F_{2,H} - R^S_{2,H}$ measured from ^{13}CH$_3$ methyl groups (*x*-axis) with $R^F_{2,H}$ obtained via scheme 1 (c, $L_1 + L_3$) or scheme 2 (d, $L_1 - L_3$) of Figure 4b. (e,f) As in (c,d) but measured on MSG. S^2_{axis}(^{2}H) was derived from R(^{13}CHD$_2$) measurements.[13] See text for the parameters of methyl geometry used to obtain ^{1}H relaxation-derived values of S^2_{axis}. Best-fit parameters from linear regression of the data are shown for each plot along with Pearson correlation coefficients, *R*, obtained for the number of data points (methyl groups) indicated in parentheses. The line $y = x$ is drawn on plots c−f.

protein L (Figure 5c,d where $R^F_{2,H}(L_1 + L_3)$ and $R^F_{2,H}(L_1 - L_3)$ are measured, respectively) and {U-[^{15}N,^{2}H], Ileδ1-[^{13}CH$_3$], Leu,Val-[^{13}CH$_3$,^{12}CD$_3$]}-MSG (Figure 5e, $R^F_{2,H}(L_1 + L_3)$; Figure 5f, $R^F_{2,H}(L_1 - L_3)$). Correlations between the sets of S^2_{axis} values are high, very similar to what has been observed between ^{13}C- and ^{2}H-derived order parameters measured in MSG recently.[13] Of interest, S^2_{axis} values obtained from $R^F_{2,H}(L_1 + L_3) - R^S_{2,H}$ are ever so slightly lower than the corresponding values from $R^F_{2,H}(L_1 - L_3) - R^S_{2,H}$, as expected from the (small) way in which external protons contribute to relaxation in each of the two cases (see eq 5).

It should be noted that, in applications involving protein L at temperatures much higher than 5 °C (i.e., for correlation times less than approximately 10 ns), the agreement between ^{2}H- and ^{1}H-derived measures of order breaks down, with values of S^2_{axis} from ^{1}H relaxation surprisingly increasing with temperature. This trend has been noted in our previous studies of methyl (^{13}CH$_3$) side-chain dynamics, where we focused on intra-methyl cross-correlation effects between ^{1}H−^{13}C and ^{1}H−^{1}H dipolar interactions as a probe of motion.[40] Specifically, in studies of protein L at 5 °C (τ_C = 10 ns), 15 °C (τ_C = 6.7 ns), 25 °C (τ_C = 5.0 ns), and 35 °C (τ_C = 3.3 ns), the pairwise root-mean-square deviation between S^2_{axis} values obtained from the approach described here and ^{2}H-based methods increases from 0.03 to 0.06 to 0.09 to 0.22, respectively. Certainly, (a small) part of the difference reflects the fact that, for lower values of τ_C, additional terms must be included in eq 4. However, the deviations are larger than expected from theory. We also note in passing that errors in S^2_{axis} values are also obtained from the quantification of experiments measuring the buildup of double-quantum coherence that results from differential ^{1}H relaxation effects,[28,29] and that depends on a function of the form $\exp(-R^F_{2,H}\,T) - \exp(-R^S_{2,H}T)$. In fact, it is only when $R^F_{2,H}$, $R^S_{2,H}$ values are measured in separate experiments (i.e., via single exponential decays) that agreement with ^{2}H-based measures of dynamics are obtained. We are currently exploring these remaining questions in more detail.

As a final point, it is of interest to compare the relative sensitivities of the schemes of Figure 4 with the sensitivity of a regular HMQC sequence that is used to obtain methyl ^{1}H, ^{13}C correlations in highly deuterated proteins.[48] In HMQC spectra recorded on large systems, the coherence pathway that transfers fast-relaxing ^{1}H magnetization to fast-relaxing multiple-quantum coherence and back to rapidly decaying proton signal contributes little to the final data set, so that essentially what is observed derives from the slowly relaxing pathway. The scheme of Figure 4a is based on an HMQC that includes a filter element to specifically select for the slowly decaying component. Thus, the signal-to-noise ratio of correlations in spectra recorded with the sequence of Figure 4a (T = 0) approaches that of regular HMQC spectra for applications involving high-molecular-weight proteins. It can be shown that, for studies of large proteins and neglecting relaxation during the τ_a,τ_b delays, the scheme of Figure 4b is reduced in sensitivity by a factor of 4 relative to the experiment of Figure 4a. In practice, however, the losses tend to be significantly higher, since for the experiment that measures $R^F_{2,H}$, it is the rapidly relaxing multiple-quantum elements, present during the intervals between *a* and *c* in Figure 4b (scheme 1) and between *a* and *b* and *d* and *e* (Figure 4b, scheme 2), that give rise to the observed signal and relaxation decay during these delays is significant. Thus, in studies of protein L, intensities of correlations measured for experiments recorded with the sequences of Figure 4a,b are in the ratio of 4.3 ± 0.7 (i.e., intensities of experiment of Figure 4a/corresponding intensities of experiment of Figure 4b), while for MSG, the ratio increases to 13.1 ± 3.1, on average. It is clear that what limits the methodology is the inherent sensitivity of spectra that quantify $R^F_{2,H}$. These spectra have sensitivities that are approximately a factor of 2−3-fold lower than those recorded with schemes that measure ^{2}H transverse relaxation in ^{13}CHD$_2$-labeled samples of MSG (for Val and Leu residues). In addition, the resolution in F_2 is degraded in data sets that measure $R^F_{2,H}$ since both fast and slowly relaxing components of magnetization are present at the start of detection, leading to cross-peaks with broad baselines. This accounts for the lower number of correlations that could be reliably quantified in the present study (~50% of the total number of Ile(δ1), Leu, and Val methyl groups relative to 80% in the case of the ^{2}H study[20]).

Concluding Remarks. A number of experimental methods have been described for measuring methyl side-chain order in $^{13}CH_2D$- and $^{13}CH_3$-labeled, highly deuterated proteins. The approaches exploit differences in ^1H relaxation rates of degenerate transitions that in turn report on specific intra-methyl dipolar cross-correlation effects related directly to S^2_{axis}. Order parameters quantifying the amplitudes of motion of Ile(δ1), Leu, and Val methyl groups obtained from ^1H-based experiments on {U-[^{15}N,^2H], Ileδ1-[$^{13}CH_3$], Leu,Val-[$^{13}CH_3$,$^{12}CD_3$]}-MSG are in good agreement with those from ^2H and ^{13}C relaxation studies ($\tau_C \approx 50$ ns); a similar level of agreement with ^2H-derived S^2_{axis} values is observed in applications involving {U-[^{15}N,^2H], Ileδ1-[$^{13}CH_3$], Leu,Val-[$^{13}CH_3$,$^{12}CD_3$]}-protein L at 5 °C ($\tau_C \approx 10$ ns). A good correlation is also observed between S^2_{axis}(^1H) and S^2_{axis}(^2H) for Ile(δ1) methyls, as measured on a {U-[^{15}N,^2H], Ileδ1-[$^{13}CH_2D$]}-MSG sample. For both $^{13}CH_3$-(Ile, Leu, Val)- and $^{13}CH_2D$-(Ile)-based probes of dynamics considered here, simulations and experiments suggest that ^1H-derived measures of order are robust for $\tau_C > 10$ ns and for applications involving highly deuterated samples. Nevertheless, ^2H relaxation experiments have a number of decided advantages. First, the relaxation of as many as five density elements can be studied to increase confidence in the extracted motional parameters. By contrast, S^2_{axis} values are obtained from only a single measure in the case of the ^1H experiments. In addition, since only one ^1H rate is measured, the data must be interpreted under the assumption that the contribution to relaxation from τ_f is negligible (i.e., $\tau_f = 0$). No such assumption is necessary in the case of ^2H or ^{13}C relaxation studies. Nevertheless, the work described here points to the high level of consistency between different measurements, further corroborating the reliability of the derived dynamics parameters. In a series of recent papers, our laboratory has shown how the rich cross-correlated spin relaxation network in methyl groups can be used to probe molecular structure and dynamics in proteins.[34,53] The present work provides yet another such example.

Acknowledgment. This work was supported by a grant from the Canadian Institutes of Health Research (CIHR) to L.E.K., who also holds a Canada Research Chair in Biochemistry. V.T. acknowledges financial support in the form of a postdoctoral fellowship from CIHR. The authors thank Dr. V. Kanelis (Hospital for the Sick Children, Toronto) for providing the sample of protein L and Dr. J. E. Ollerenshaw (University of Toronto) for computer simulations and helpful discussions.

Supporting Information Available: Tables listing all spectral density terms that contribute to $R^F_{2,H} - R^S_{2,H}$ in isolated $^{13}CH_2D$ and $^{13}CH_3$ methyl groups. This material is available free of charge via the Internet at http://pubs.acs.org.

JA060817D

(51) Shaka, A. J.; Keeler, J.; Frenkiel, T.; Freeman, R. *J. Magn. Reson.* **1983**, *52*, 335−338.
(52) Marion, D.; Wüthrich, K. *Biochem. Biophys. Res. Commun.* **1983**, *113*, 967−974.
(53) Tugarinov, V.; Hwang, P. M.; Kay, L. E. *Annu. Rev. Biochem.* **2004**, *73*, 107−146.